Check for updates

Multiple bonding in unbridged Mn–Mn dimers of solid-state nitridomanganate(IV) oxide Ca6[Mn2N6]O

Niklas Buschmann,[a] Dominik Werhahn,[a] Simon Steinberg, [b] Clemens Ritter,[c] J. Paul Attfield [d] and Simon D. Kloß [*a]

Unbridged metal–metal bonding is rare in solid-state materials owing to preferred coordination of metals through main group anions. Here, we present a calcium nitridomanganate(IV) oxide Ca6[Mn2N6]O with [MnN3]2 dimers prepared by hot isostatic pressing. This preparation opens the possibility to study unbridged metal–metal dimer systems in solid-state materials.

Unbridged metal–metal bonded clusters have been widely studied in inorganic complex and cluster chemistry since F. A. Cotton reported the first instances of quadruple bonding in the famous octachloridodirhenate(III) anions $[Re_2Cl_8]^{2-}$.[1,2] This discovery triggered a search for similar dinuclear and multinuclear cluster compounds that advanced the fundamental understanding of their chemistry and electronic properties, *e.g.* multiple metal–metal bonding with high bond orders of 4–6 and the exchange mechanisms of delocalized electrons.[3–6] Simultaneously, a series of properties and applications arose like single-molecule magnetic behaviour shown in a triiron cluster with $S = 11/2$ ground state,[7] and small molecule activation of *e.g.* H_2, CO_2 and N_2, as well as C–H and C–F bonds.[8–10]

The multitude of homo- and heterometallic dimers found in molecular compounds vastly overwhelms the number of classical solid-state materials featuring such moieties. There, unbridged metal–metal bonding occurs, next to trivial cases of metals and intermetallics, in subvalent systems bordering on interstitials such as the Cs suboxides and in clusters of valence electron poor metals such as the Chevrel-phases like superconducting $PbMo_6S_8$.[11,12] These systems feature either extended intermetallic frameworks or larger polycationic clusters to alleviate the electron-poor configurations of the constituting transition metals. Dimers

with unbridged metal–metal interactions are found in covalent systems such as chalkogenidetetrelates $A_6[Tt_2X_6]$ with A = Na, K, Cs, Tt = Si, Ge, Sn and X = S, Se, Te as well as in reduced nitridotetrelates $AESi_6N_8$ (AE = Sr, Ba) with $[SiN_3]_2$ dimers and $AE_6Ge_2N_6$ with $[GeN_3]_2$ dimers.[13–20] In 3d nitridometallates, the only reports of unbridged dimers were on nitridomanganates $Li_6AE_2[Mn_2N_6]$ (AE = Ca, Sr) and the nitridochromate hydride $Ca_6[Cr_2N_6]H$, while for nitridochromates $AE_4[Cr_2N_6]$ (AE = Ca, Sr) and $Li_4Sr_2[Cr_2N_6]$ a Cr–Cr interaction was reported across the edge of bow-tie double tetrahedra.[21–25]

The preparation of the nitridomanganates has classically been achieved using ambient pressure N_2 gas flow synthesis methods. These work well for early transition metal nitrides as shown by numerous compounds in the AE/Ln/Ac-Mn-N system such as the AE_3MnN_3 and the $(Ln_2, Ac_2)MnN_3$ (Ln/Ac = Ce, Th, U) family of materials and $Li_6AE_2[Mn_2N_6]$ (AE = Ca, Sr).[22,26–29] High-pressure methods, however, such as multianvil large-volume-presses with pressures in the gigapascal range were recently demonstrated to stabilize transition metal nitrides in high oxidation states such as Ca_4FeN_4, Ca_2NiN_2, or nitride perovskite-types such as $LaReN_3$ and Ln_2ReN_4.[30–33] The drawback of multianvil synthesis is small sample volumes, which make scale-up of potentially useful materials difficult. Hot isostatic pressing (HIP) on the other hand feature large sample volumes and static dinitrogen pressures in the megapascal range (usually up to 200 MPa N_2). Such systems allow scale-up and have already been successfully implemented for industrial relevant luminescent main group nitrides such as $Ca_2PN_3:Eu^{2+}$, zeolite-type $AE_3P_5N_{10}X:Eu^{2+}$ (AE = Sr, Ba; X = Cl, Br), and $Sr_2[BeAl_3N_5]:Eu^{2+}$.[34–36] Nitridometallate synthesis, however, was never reported using a HIP, only the preparation of interstitial nitrides like Fe_3W_3N and Fe_6W_6N.[37]

Here, we present the preparation of the calcium nitrido-manganate(IV) oxide $Ca_6[Mn_2N_6]O$ using a hot-isostatic press through a two-step reaction of calcium nitride Ca_3N_2 (3.1 eq.) and manganese nitride $Mn_6N_{5.26}$ (1 eq.).

The first reaction step was carried out at 150 MPa of static N_2 pressure and 1100 °C for 10 h, then the product was ground and

[a] Department of Chemistry, LMU Munich, Butenandtstr. 5-13, 81377 Munich, Germany. E-mail: simon.kloss@cup.lmu.de

[b] Institute of Inorganic Chemistry, RWTH Aachen, Melatener Str. 2, 52074 Aachen, Germany

[c] Institut Laue-Langevin, Grenoble, France

[d] University of Edinburgh, Centre for Science at Extreme Conditions and School of Chemistry, Edinburgh EH9 3FD, UK
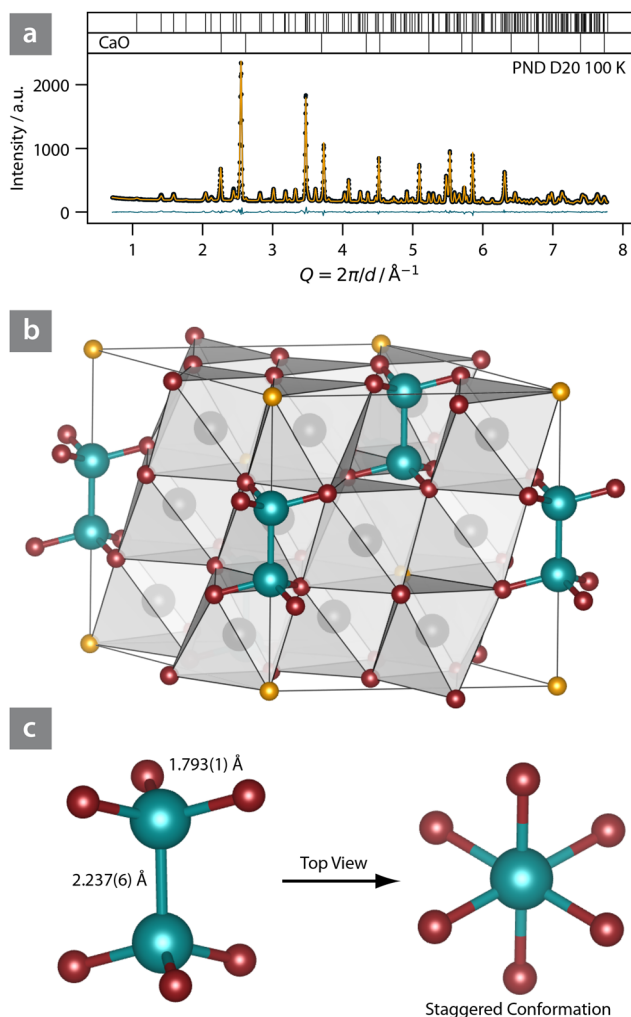
Fig. 1 (a) Powder neutron diffraction pattern obtained at 100 K at the D20 beamline of the ILL. Rietveld refinement in orange against collected datapoints (black) with difference curve in blue and Bragg positions as black vertical lines. The CaO byproduct amounts to 1 wt%. (b) Structure of $Ca_6[Mn_2N_6]O$ with Ca in black (polyhedra), Mn in blue, N in red and O in orange. (c) $[MnN_3]_2$ dimer with metal–metal and metal-N interatomic distances highlighted. The staggered ligand conformation is highlighted on the right side.

heated at 150 MPa (N_2) and 1300 °C for 20 h (detailed conditions in SI). A two-step process was necessary as single-step reactions at 1100 °C led to formation of the known phase Ca_6MnN_5, while at 1300 °C the known Ca_3MnN_3 was obtained.[28,38] $Ca_6[Mn_2N_6]O$ was obtained as a black powder in high purity, sometimes with a small CaO by-product (*ca.* 1–4 wt%). The oxygen necessary for product formation likely stems from water and oxygen impurities in the nitrogen pressure gas used to run the HIP, phase formation was also observed when CaO was used as additional oxygen source.

Energy dispersive X-ray spectroscopy in a scanning electron microscope was used to determine metal ratios (measured: Ca/Mn = 2.9(1)), while nitrogen content could not be determined due to rapid hydrolysis of $Ca_6[Mn_2N_6]O$ (Table S1).

The structure of $Ca_6[Mn_2N_6]O$ (SG $R\bar{3}$, no. 148) was refined on powder X-ray diffraction data (300 K, Fig. S2) and powder

neutron diffraction (PND) data (100 K, ILL D20 beamline, Fig. 1a) starting from the structure model of $Ca_6[Ge_2N_6]$ after initial indexing indicated a similar structure (details in SI).[20] An additional oxide anion position was found *via* difference Fourier analysis and confirmed by PND. The structure of $Ca_6[Mn_2N_6]O$ is isotypic to calcium nitridochromate hydride $Ca_6[Cr_2N_6]H$ and can best be described as a rhombohedral substitution derivative of the NaCl-type. The N/O to Ca/Mn_2 ratio is 1:1, resulting in a cubic dense packing of N/O anions where Ca and Mn_2 dimers occupy all octahedral voids (Fig. 1b).

The $[MnN_3]_2$ dimers enter a staggered conformation of N ligands (Fig. 1c) where the Mn–N interatomic distance (d = 1.793(1) Å) is similar to Mn–N interatomic distances report for other compounds with threefold coordination of Mn such as $Ba_3Mn^{III}N_3$ (d = 1.738 Å), $Ca_3Mn^{III}N_3$ (d = 1.793 Å), $Ca_6Mn^{III}N_5$ (d = 1.757 Å).[28,29,38] In $Ca_6[Mn_2N_6]O$, manganese is in the formal oxidation state of +IV leaving three unpaired electrons available for Mn–Mn multiple bonding. The Mn–Mn bond length is 2.237(6) Å, which is shorter than the reported bond length in the only other nitridomanganates with $[MnN_3]_2$ dimers, *i.e.* $Li_6AE_2[Mn_2^{IV}N_6]$ with AE = Ca (d = 2.357 Å) and Sr (d = 2.536 Å).[21,22] DFT-based analysis of Mn–Mn bonded dimer complexes showed that an interatomic distance of 2.237(6) Å corresponds to a bond order in the range of 1.5 to 2.[39] To provide an insight into the bond order of the herein reported material, we also completed DFT-based computations whose results are provided below.

The Ca–N/O interatomic distances (d_N = 2.453(2)–2.626(2) Å, d_O = 2.512(2) Å, Table S4) are in line with other reports of Ca in octahedral coordination of similar compounds such as Ca_4FeN_4 (d = 2.43–2.82 Å) and $Li_6Ca_2[Mn_2N_6]$ (d = 2.51–2.63 Å).[21,31] Bond valence sum calculations performed for the CaN_5O octahedra resulted in a valence of 2.04 for Ca (R_0(Ca–N) = 2.14 Å, R_0(Ca–O) = 1.967 Å) indicating predominantly ionic interactions.[40] Tentative calculations for Mn yielded a valence of 3.3, which however is probably not meaningful due to the Mn–Mn bonding as well as the lack of suitable R_0 values for nitridomanganates(IV).

The oxide anion is sixfold-coordinated by Ca in OCa_6 octahedra. Interatomic distances d_{Ca-O} = 2.512(2) Å are longer than values found CaO (d = 2.390 Å).[41] However, OM_6 octahedra in other nitride oxides such as $Ho_3[PN_4]O$ were previously reported also to have longer M–O distances, which may be owed to electrostatic repulsion between adjacent metal centres.[42] Enlarged isotropic displacement parameters of O detected in the PXRD measurements (higher Q-resolution than PND) reflect the larger volume of the coordination polyhedron (Table S6). Refined occupancies from neutron and X-ray diffraction data are in line with the presence of oxide.

The magnetic susceptibility of $Ca_6[Mn_2N_6]O$ was collected at 30 kOe in the range of 2 to 300 K, while field dependent magnetization was collected at 300 and 2 K in the range H = ±50 kOe (Fig. 2 and Fig. S3). The susceptibility shows a small temperature-dependence, in line with the magnetization data, stemming from a paramagnetic contribution as well as a temperature-independent term. A fit in the range
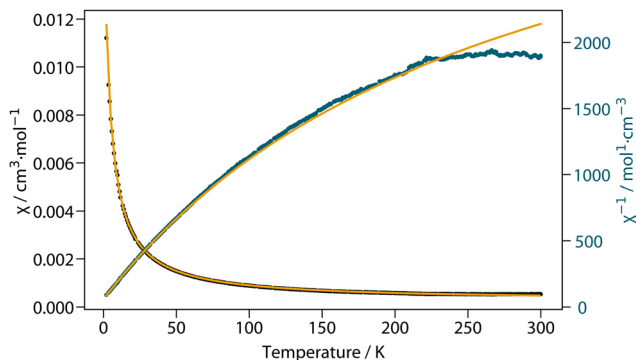
ChemComm

Fig. 2 Magnetic (inverse: blue) susceptibility of $Ca_6[Mn_2N_6]O$. A Curie-Type fit is shown in orange.

$2 \leq T \leq 300$ K as $X = X_{TIP} + \dfrac{C}{T}$ yielded a temperature independent susceptibility of $X_0 = 2.45(2)\ 10^{-4}$ cm^3 mol^{-1} and an effective magnetic moment $\mu_{eff} = 0.52(1)\mu_B$. In unbridged metal dimers, strong direct exchange interaction leads to antiferromagnetic alignment of spins, which is in agreement with metal–metal bonding. For such moieties, a van Vleck-type temperature-independent paramagnetism (TIP) stems from low-lying excited states, as reported for molecular species such as a Cr_2 dimer ($X_{TIP} = 1.12(5) \cdot 10^{-4}$ cm^3 mol^{-1}) and also for a solid-state compound $Li_4Sr_2[Cr_2N_6]$ ($X_{TIP} = 1.34 \cdot 10^{-4}$ cm^3 mol^{-1}).[4,25] The small temperature-dependent term may arise from impurities that are not visible in the powder diffraction patterns (e.g. 1.8% of a $S = 3/2$, Mn^{4+}, impurity), as similarly suggested for molecular compounds in the solid-state.[43]

Temperature-dependent magnetism that increases towards higher temperatures owed to increasing population of low-lying excited states is indicated by the discrepancy in fitted and measured data at $T > 200$ K. Such behaviour was observed, for example, for chromium(II) trifluoromethanecarboxylates

with Cr_2 dimers.[44] The Curie-type impurity, however, impeded further analysis.

The structural behaviour of $Ca_6[Mn_2^{IV}N_6]O$ at high temperatures was studied with temperature-dependent powder X-ray diffraction up to 900 °C (Fig. S4a). There is a visible deterioration of reflection intensities and position shifts starting at ca. 800 °C, which may indicate decomposition or phase transition of the material. The thermal expansion of $Ca_6[Mn_2N_6]O$ was investigated from lattice parameters extracted with Rietveld-fits (Fig. S4b). Both lattice parameters, a and c, show positive thermal expansion with coefficients $\alpha_a = 17.0(4)\ 10^{-6}$ K^{-1}, $\alpha_c = 16.3(2)\ 10^{-6}$ K^{-1} and $\alpha_V = 5.08(7)\ 10^{-5}$ K^{-1}. The expansion parameters are similar to other observed transition metal nitrides such as Ca_2NiN_2 ($\alpha_V = 4.3(2)\ 10^{-5}$ K^{-1}, Ln_2ReN_4 (Ln = Pr, Nd) and $LaReN_3$.[30,31,33]

Electronic structure analysis of $Ca_6[Mn_2N_6]O$ was completed using density-functional-theory-based techniques (see SI for further technical details). The Mulliken charges as well as the small ICOBI values indicate ionic Ca–O and Ca–N interactions (Fig. 3), while the character of the Mn–N bonds should be depicted as polar-covalent. The Mn–N bonds are largely based on the N p and the Mn d_{xy} and $d_{x^2-y^2}$ orbitals, while the remaining Mn d orbitals are involved in Mn–Mn multiple bonding. The modest dispersion corresponding to Mn d bands means that the electrons are rather located within the Mn–Mn multiple bonds, while the Mn–Mn ICOBI value of 1.505 agrees with the bond orders previously determined for Mn–Mn bonds of complexes (1.5 to 2).[39] The π-type character is also mirrored by the LUMO of a Mn_2N_6 unit shown in Fig. 3c; however, adding further electrons to such a unit would result in a higher population of antibonding states resulting in an electronically unfavourable situation. Therefore, it may be inferred that this particular type of electronic configuration is reached for the Mn–Mn dimers in order to optimize the bonding scenario. The staggered conformation of the Mn_2N_6 dimers may be due to
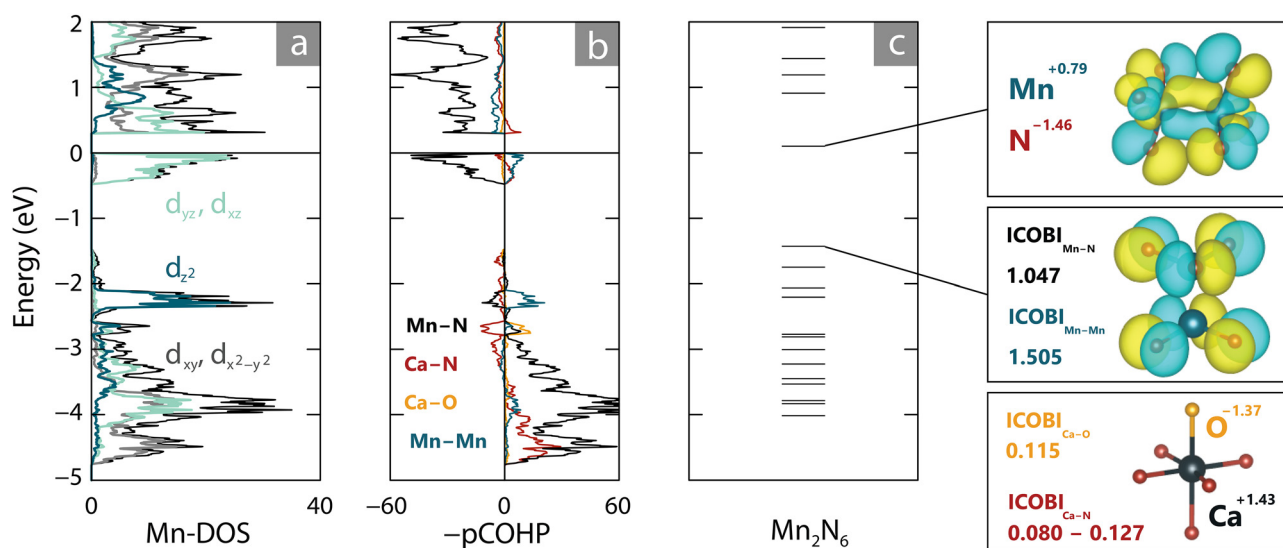

Fig. 3 (a) Mn partial- and orbital-projected densities of states (DOS). (b) projected crystal orbital Hamilton population (pCOHP). (c) MO diagram and representations showing the HOMO and LUMO of a Mn_2N_6 unit. The Mulliken charges and ICOBI/bond values have been included in the insets.

repulsion of the nitride anions and in contrast to the ecliptic conformation in $[Re_2Cl_8]^{2-}$ anions.

The preparation of unbridged Mn–Mn dimers in solid-state materials under thermodynamic conditions is remarkable owing to the preference for coordination by main group anions. In complex chemistry, such arrangements usually are kinetically stabilized through sterically active ligands. Here, we showed that the Mn_2 dimer in $Ca_6[Mn_2N_6]O$ has a bond order of 1.5. Magnetization measurements revealed a temperature independent paramagnetism indicating low-lying excited states. The preparation of $Ca_6[Mn_2N_6]O$ using a hot isostatic press enables further research on transition metal nitrides with metal–metal contacts by for example interchanging electropositive cations to tune the M–M distance or interchanging metals and anions to create heterovalent systems featuring interesting magnetic phenomena.

Conflicts of interest

There are no conflicts to declare.

Data availability

Supplementary information: Details on methods, powder X-ray diffraction, powder neutron diffraction, structure model, energy dispersive X-ray spectroscopy, further magnetic measurements, and temperature dependent powder X-ray diffraction. See DOI: **https://doi.org/10.1039/d5cc04348d**. Raw data for this article, including magnetic and powder diffraction data are available at LMU Open Data at **https://doi.org/10.5282/ubm/data.674**.

CCDC 2477089 and 2477090 contain the supplementary crystallographic data for this paper.[45a,b]

Notes and references

1 F. A. Cotton and C. B. Harris, *Inorg. Chem.*, 1965, **4**, 330–333.
2 F. A. Cotton, N. F. Curtis, C. B. Harris, B. F. Johnson, S. J. Lippard, J. T. Mague, W. R. Robinson and J. S. Wood, *Science*, 1964, **145**, 1305–1307.
3 J. F. Berry and C. C. Lu, *Inorg. Chem.*, 2017, **56**, 7577–7581.
4 T. Nguyen, A. D. Sutton, M. Brynda, J. C. Fettinger, G. J. Long and P. P. Power, *Science*, 2005, **310**, 844–847.
5 P. W. Anderson and H. Hasegawa, *Phys. Rev.*, 1955, **100**, 675–681.
6 F. R. Wagner, A. Noor and R. Kempe, *Nat. Chem.*, 2009, **1**, 529–536.
7 R. Hernandez Sanchez, A. K. Bartholomew, T. M. Powers, G. Menard and T. A. Betley, *J. Am. Chem. Soc.*, 2016, **138**, 2235–2243.
8 Q. Wang, S. H. Brooks, T. Liu and N. C. Tomson, *Chem. Commun.*, 2021, **57**, 2839–2853.
9 K. M. Gramigna, D. A. Dickie, B. M. Foxman and C. M. Thomas, *ACS Catal.*, 2019, **9**, 3153–3164.
10 R. M. Charles and T. P. Brewster, *Coord. Chem. Rev.*, 2021, **433**, 213765.
11 A. Simon, *Angew. Chem., Int. Ed.*, 2003, **27**, 159–183.
12 B. T. Matthias, M. Marezio, E. Corenzwit, A. S. Cooper and H. E. Barz, *Science*, 1972, **175**, 1465–1466.
13 G. Dittmar, *Angew. Chem., Int. Ed.*, 2003, **16**, 554.
14 B. Eisenmann, J. Hansa and H. Schäfer, *Mater. Res. Bull.*, 1985, **20**, 1339–1346.
15 G. Dittmar, *Z. Anorg. Allg. Chem.*, 2004, **453**, 68–78.
16 B. Eisenmann, E. Kieselbach, H. Schäfer and H. Schrod, *Z. Anorg. Allg. Chem.*, 2004, **516**, 49–54.
17 B. Friede and M. Jansen, *Z. Naturforsch. B*, 1999, **54**, 1095–1098.
18 F. Stadler, O. Oeckler, J. Senker, H. A. Höppe, P. Kroll and W. Schnick, *Angew. Chem.*, 2005, **117**, 573–576.
19 F. Stadler and W. Schnick, *Z. Anorg. Allg. Chem.*, 2007, **633**, 589–592.
20 L. Link, M. Pathak, F. Jach, P. Koželj, A. Ormeci, P. Höhn and R. Niewa, *Angew. Chem.*, 2021, **133**, 7769–7774.
21 O. Hochrein, Y. Grin and R. Kniep, *Angew. Chem., Int. Ed.*, 1998, **37**, 1582–1585.
22 O. Hochrein, P. Höhn and R. Kniep, *Z. Anorg. Allg. Chem.*, 2003, **629**, 923–927.
23 M. S. Bailey and F. J. DiSalvo, *Dalton Trans.*, 2003, 2621–2625.
24 M. S. Bailey, M. N. Obrovac, E. Baillet, T. K. Reynolds, D. B. Zax and F. J. DiSalvo, *Inorg. Chem.*, 2003, **42**, 5572–5578.
25 O. Hochrein, M. Kohout, W. Schnelle and R. Kniep, *Z. Anorg. Allg. Chem.*, 2002, **628**, 2738–2743.
26 R. Benz and W. H. Zachariasen, *J. Nucl. Mater.*, 1970, **37**, 109–113.
27 R. Niewa, G. V. Vajenine, F. J. DiSalvo, H. Luob and W. B. Yelon, *Z. Naturforsch. B*, 1998, **53**, 63–74.
28 A. Tennstedt, C. Röhr and R. Kniep, *Z. Naturforsch. B*, 1993, **48**, 1831–1834.
29 A. Tennstedt, C. Röhr and R. Kniep, *Z. Naturforsch. B*, 1993, **48**, 794–796.
30 S. D. Kloß and J. P. Attfield, *Chem. Commun.*, 2021, **57**, 10427–10430.
31 S. D. Kloß, A. Haffner, P. Manuel, M. Goto, Y. Shimakawa and J. P. Attfield, *Nat. Commun.*, 2021, **12**, 571.
32 S. D. Kloß, C. Ritter and J. P. Attfield, *Z. Anorg. Allg. Chem.*, 2022, 648.
33 M. Weidemann, D. Werhahn, C. Mayer, S. Kläger, C. Ritter, P. Manuel, J. P. Attfield and S. D. Kloß, *Nat. Chem.*, 2024, **16**, 1723–1731.
34 S. Wendl, S. Mardazad, P. Strobel, P. J. Schmidt and W. Schnick, *Angew. Chem., Int. Ed.*, 2020, **59**, 18240–18243.
35 S. Wendl, M. Zipkat, P. Strobel, P. J. Schmidt and W. Schnick, *Angew. Chem., Int. Ed.*, 2020, **60**, 4470–4473.
36 E. Elzer, P. Strobel, V. Weiler, P. J. Schmidt and W. Schnick, *Chem. Mater.*, 2020, **32**, 6611–6617.
37 T. Waki, S. Terazawa, Y. Tabata, Y. Murase, M. Kato, K. Hirota, S. Ikeda, H. Kobayashi, K. Sato, K. Kindo and H. Nakamura, *J. Alloys Compd.*, 2011, **509**, 9451–9455.
38 D. H. Gregory, M. G. Barker, P. P. Edwards and D. J. Siddons, *Inorg. Chem.*, 2002, **34**, 5195–5198.
39 F. Hujon, R. H. Duncan Lyngdoh and R. B. King, *New J. Chem.*, 2020, **44**, 12993–13006.
40 N. E. Brese and M. O'Keeffe, *Acta Crystallogr., Sect. B*, 1991, **47**, 192–197.
41 W. Gerlach, *Z. Phys.*, 1922, **9**, 184–192.
42 S. D. Kloß, N. Weidmann and W. Schnick, *Eur. J. Solid State Inorg. Chem.*, 2017, **2017**, 1930–1937.
43 F. A. Cotton, H. Chen, L. M. Daniels and X. Feng, *J. Am. Chem. Soc.*, 2002, **114**, 8980–8983.
44 C. J. Bilgrien, R. S. Drago, C. J. O'Conno and N. Wong, *Inorg. Chem.*, 2002, **27**, 1410–1417.
45 (*a*) N. Buschmann, D. Werhahn, S. Steinberg, C. Ritter, J. P. Attfield and S. D. Kloß, CCDC 2477089: Experimental Crystal Structure Determination, 2025, DOI: **10.5517/ccdc.csd.cc2p4m3l**; (*b*) N. Buschmann, D. Werhahn, S. Steinberg, C. Ritter, J. P. Attfield and S. D. Kloß, CCDC 2477090: Experimental Crystal Structure Determination, 2025, DOI: **10.5517/ccdc.csd.cc2p4m4m**.